Supplementary Information

A Marine Bacterium-Inspired Electrochemical Regulation for Continuous Uranium Extraction from Seawater and Salt Lake Brine

Linsen Yang,[a] Yongchao Qian,[a] Zhehua Zhang,[a, b] Tingyang Li,[a, b] Xiangbin Lin,[a, b] Lin Fu,[a, b] Shengyang Zhou,[a] Xiang-Yu Kong[a, b], Lei Jiang [a, b] & Liping Wen*[a, b]

[a] CAS Key Laboratory of Bio-inspired Materials and Interfacial Science, Technical Institute of Physics and Chemistry, Chinese Academy of Sciences, Beijing 100190, P. R. China.

[b] School of Future Technology, University of Chinese Academy of Sciences, Beijing 100049, P. R. China.

Correspondence and requests for materials should be addressed to L. Wen (e-mail: wen@mail.ipc.ac.cn).

Table of Contents

Supplementary Methods

Synthetic procedures of g-$C_{34}N_6$-COF. The synthesis of PIM-1 powder was performed according to a previously published method[1]. 3,5-dicarbonitrile-2,4,6-trimethylpyridine (34.2 mg, 0.2 mmol), 1,3,5-tris-(4-formylphenyl)triazine (78.72 mg, 0.2 mmol), and piperidine (102.16 mg, 1.2 mmol) were dispersed using 8 mL N, N-dimethylformamide in a pyrex tube with Teflon nuts. The mixture was homogenised by sonication for 15 min and then degassed using three freeze-pump-thaw cycles. The tube was heated in a 180℃ oil bath for three days. The tube was cooled to room temperature and the precipitate was collected by filtration. The mixture was washed three times with tetrahydrofuran (50 mL), methanol (50 mL), and dichloromethane (50 mL). The yellow product was then dried at 80 ℃ in a vacuum oven for 12 h.

Synthetic procedures of AO-g-$C_{34}N_6$-COF. g-$C_{34}N_6$-COF (30 mg) was dispersed in 40 ml tetrahydrofuran and sonicated in a bath sonicator for 10 min. The mixture was stirred at room temperature for 20 min and then heated to 69 ℃. A hydroxylamine solution (10 mL, 50 wt. % in H_2O) was subsequently added using a dropping funnel. The reaction mixture was refluxed for 23 h and the obtained suspension was filtered to oobtain residue, which was washed with ethanol three times. The orange-yellow product was dried at 60 ℃ in a vacuum oven for 12 h.

Electrode fabrication. AO-g-$C_{34}N_6$-COF (5 mg), carboxy-functional nanocellulose (84 mg, 1.2 wt% in H_2O, the actual solid weight was 1 mg), and 14 mg single-walled carbon nanotubes functionalized with carboxyl groups were dispersed in 20 mL N, N-dimethylformamide using an ultrasonic cell disruptor for 1 min. Then the homogeneous dispersion was vacuum-filtered on a Nylon filter membrane (0.22 μm) for 12 h. The semi-dry membrane was dried at 80 ℃ in a vacuum oven for 12 h, and the black self-standing S-COF membrane was easily separated from the filter membrane. The S-COF membrane was cut into 1 × 1 cm pieces. The weights of the square membranes ranged from 2.0 to 2.6 mg. When the current density was adjusted, the membrane was attached to graphite paper of varying areas using conductive silver adhesive. Then these electrodes were dried at 50 ℃ in an oven for use.

Material characterization. Fourier transform infrared spectra were obtained using a spectrometer (Varian Excalibur 3100) in the transmittance mode. Transmission electron microscopy (TEM) and energy dispersive spectroscopy (EDS) were performed using a JEOL JEM-2100F instrument. The morphologies were examined using scanning electron microscopy (SEM, HITACHI S-4800). The pore characteristics of the COFs were evaluated based on N_2 sorption isotherms at 77 K, as determined using a Quantachrome gas sorption analyser (Quadrasorb SI-MP). The thermal properties of the COFs were characterised using the diamond thermogravimetry-differential thermal analysis (TG-DTA) 6300 thermogravimetric analyser. UV-Vis spectra were collected using a UV-Vis spectrophotometre (Shimadzu UV-2600). The uranium concentrations in the natural seawater and salt lake brine were determined using an inductively coupled plasma-mass spectrometer (ICP-MS; PerkinElmer NexION 1000G). The electrochemical workstation used was CHI660B. The high-frequency pulses were generated using an arbitrary waveform generator (RIGOL DG1062Z).

Uranium extraction from spiked seawater. The uranium-spiked solutions were prepared by dissolving uranyl nitrate salts in natural seawater (Yellow Sea, Tsingtao, China). The natural seawater was filtered through filter membranes (0.22μm) to remove impurities and microorganisms before preparing the solutions. An S-COF membrane was used as the negative electrode, and a graphite rod (6 mm in diameter) was used as the positive electrode. Square pulses at 400 Hz with varying voltages and duty ratios were applied between the electrodes for uranium extraction.

Solution samples were collected at different intervals.

The concentrations of uranium were determined via UV-Vis absorption spectra based on the peak at 652 nm using arsenazo(III) as the chromogenic agent. The mass of uranium loaded onto the negative electrode was calculated as follows:

$m_U = (C_0 - C_t) \times m$

where m_U (g) is the mass of adsorbed uranium, C_0 (ppm) is the original concentration of the solution, C_t (ppm) is the concentration of uranium detected at a specific time point t during the extraction process, and m (g) is the total mass of the solution.

Uranium extraction from natural seawater and salt lake brine. Natural seawater was used to evaluate the uranium extraction performance of the S-COF membrane. The pH of the natural seawater was 8.09, and the salinity was ~ 3.2%. The environmental temperature was 25 °C. The S-COF membrane used as an electrode weighed 2.0 mg. Each electrode was treated with 2 L natural seawater for 24 h per treatment. The entire process lasted 21 days, and the total amount of treated seawater was 42 L. The natural salt-lake brine was obtained from the Chaerhan Salt Lake in Golmud, Northwest China's Qinghai Province. 2.0 mg membrane was used to treat 500 mL of brine for 4 days per treatment, and the whole process lasted 32 days. The total volume of brine used was 4 L. The uranium concentration was measured using ICP-MS. The natural seawater was filtered through filter membranes (0.22μm) while the salt lake brine was not filtered.

Computational calculations. The crystalline structures of the COF were determined using the Cambridge Serial Total Energy Package (CASTEP) code, which uses the generalised gradient approximation of the Perdew-Burke-Ernzerhof scheme to describe the exchange-correlation interactions[2]. For geometric optimisation, the cut-off energy was set at 500.0 eV. The convergence tolerance was set to 10^{-5} eV/atom, the maximum stress was set to 0.05 GPa, the maximum force on atoms was 0.03 eV/Å, and the ionic displacement was 10^{-3} Å. The Brillouin zone was sampled using a 1 × 1 × 4 k-point mesh in the Monkhorst-Pack scheme. The differential charge density distribution was calculated using the density-functional tight-binding (DFTB+) method. The calculations were performed using the DFTB + program package[3]. DFTB is a semi-empirical density-functional theory method based on the tight-binding approach, that can effectively reduce the complexity of the calculation.

Section S2. Supplementary figures and tables

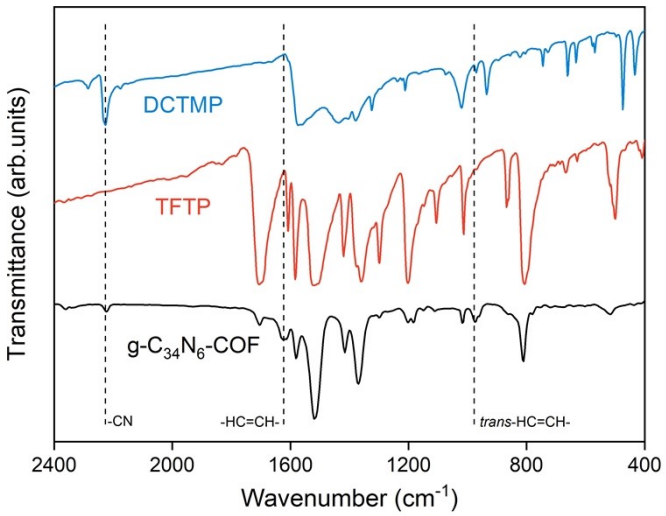

Fig. S1 FT-IR spectra of g-$C_{34}N_6$-COF and two monomers. The characteristic peak at 1627 cm^{-1} was attributed to the carbon-carbon double bond (C=C) stretching. The stretching vibration of the *trans* -HC=CH- in the fingerprint region at 975 cm^{-1} demonstrated the trans-configurations of olefin linkages. The nitrile peak at 2221 cm^{-1} came from DCTMP.

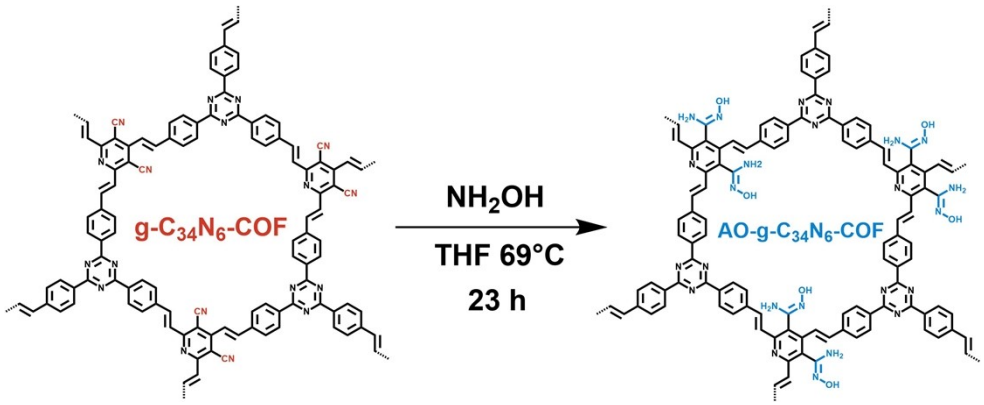

Fig. S2 Synthesis method of AO-g-$C_{34}N_6$-COF. The amidoxime groups introduced into the COF through functionalization served as specific binding sites for uranium.

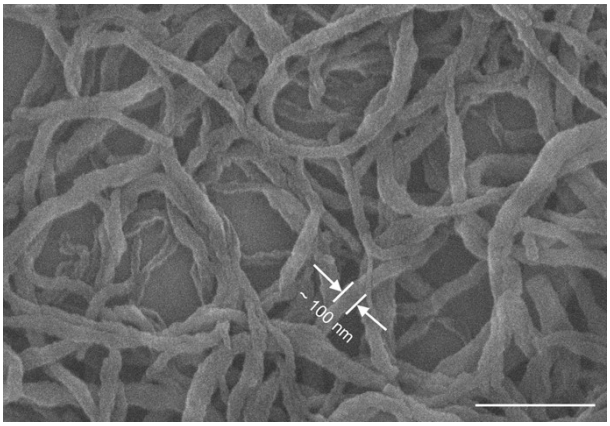

Fig. S3 SEM image of g-$C_{34}N_6$-COF. The g-$C_{34}N_6$-COF showed a fibre-like morphology with a mean diameter of ~ 100 nm. Scale bar, 500 nm.

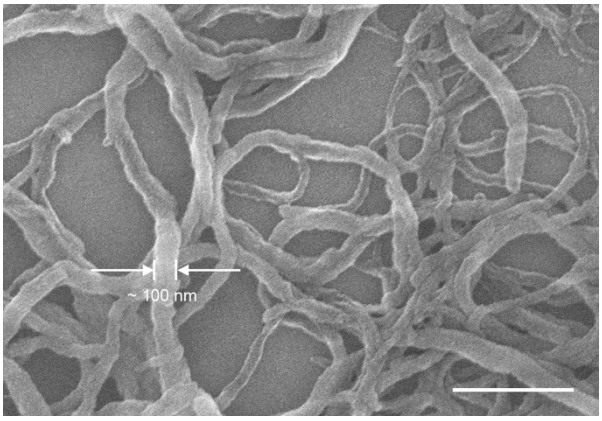

Fig. S4 SEM image of AO-g-$C_{34}N_6$-COF. The AO-g-$C_{34}N_6$-COF preserved the fibre-like morphology after amidoxime functionalization. The mean diameter is ~ 100 nm. Scale bar, 500 nm.

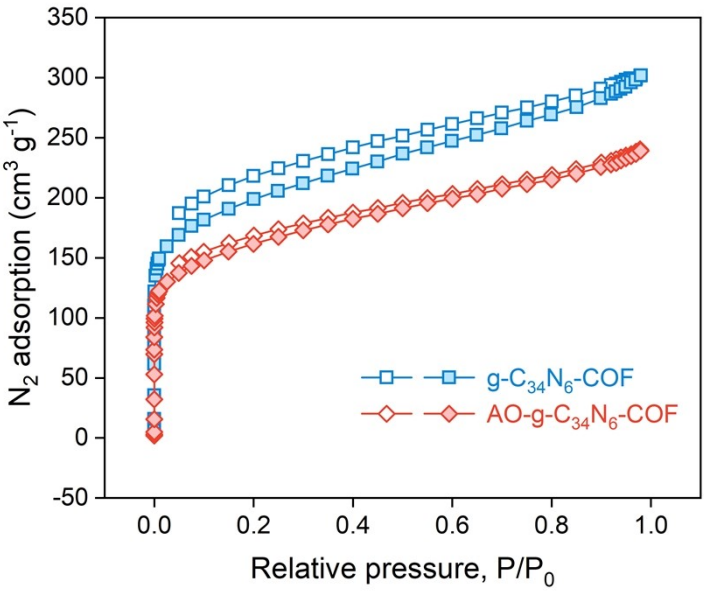

Fig. S5 N_2 adsorption/desorption isotherms of g-$C_{34}N_6$-COF and AO-g-$C_{34}N_6$-COF at 77 K. The specific surface area remained high after amidoxime functionalization.

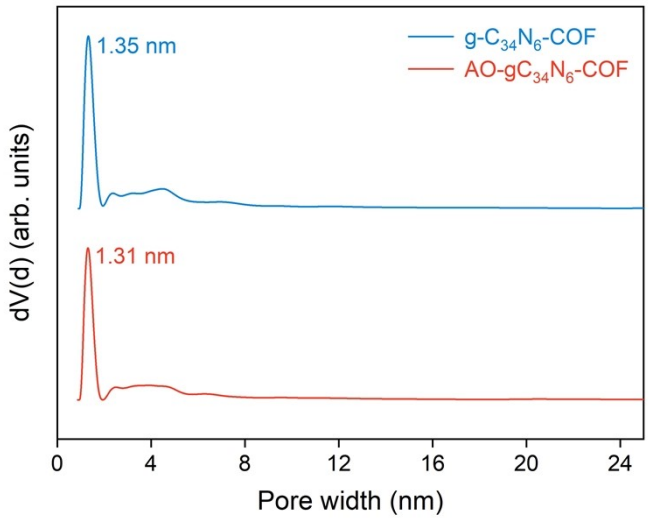

Fig. S6 Pore size distribution of g-$C_{34}N_6$-COF and AO-g-$C_{34}N_6$-COF based on N_2 adsorption and QSDFT method. The pore width reduced slightly after amidoxime functionalization.

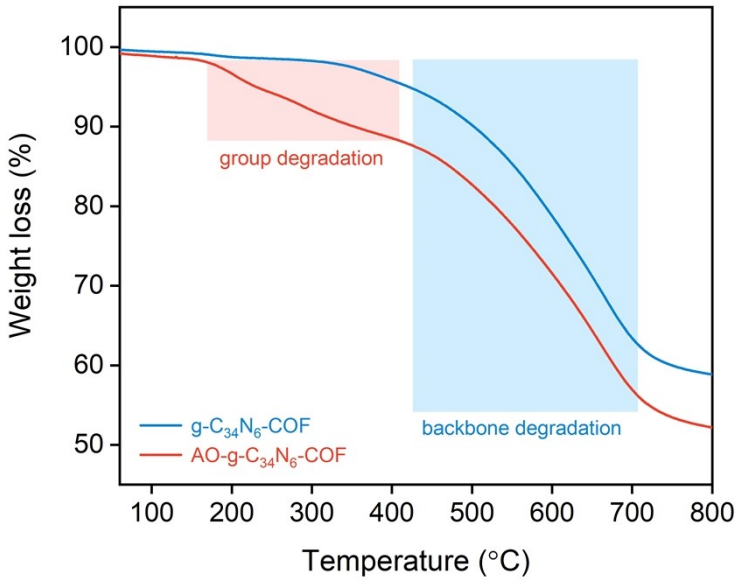

Fig. S7 TGA curves of synthetic g-$C_{34}N_6$-COF and AO-g-$C_{34}N_6$-COF based on thermal gravimetric analysis. Compared with g-$C_{34}N_6$-COF, AO-g-$C_{34}N_6$-COF had an additional step corresponding to the degradation of the amidoxime group before backbone damage.

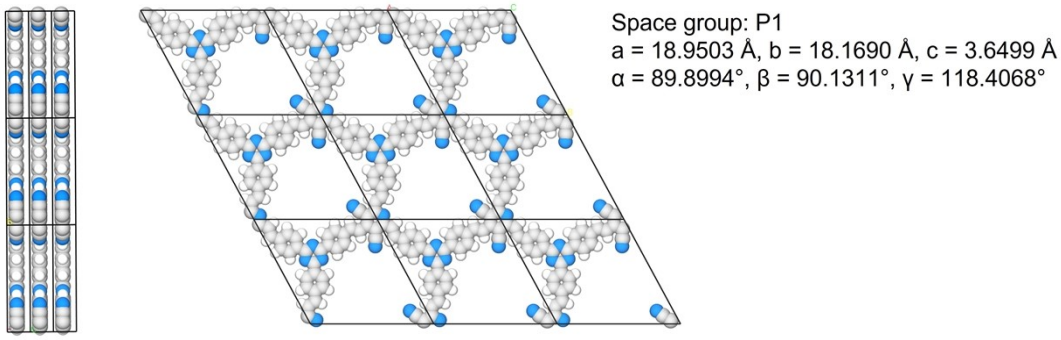

Fig. S8 Views of modeled g-$C_{34}N_6$-COF crystal structure.

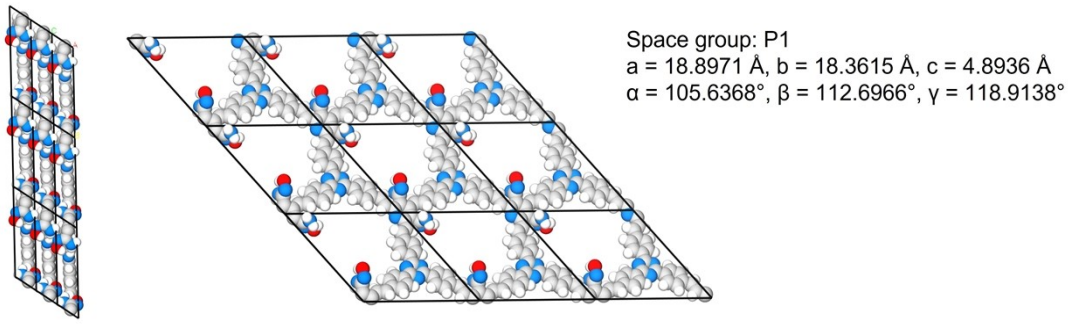

Fig. S9 Views of modeled AO-g-$C_{34}N_6$-COF crystal structure.

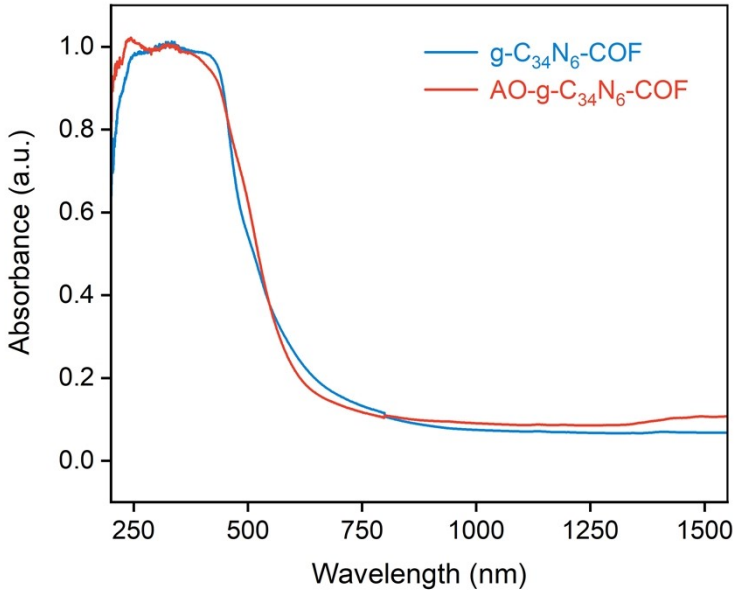

Fig. S10 UV-Vis DRS of g-$C_{34}N_6$-COF and AO-g-$C_{34}N_6$-COF. Compared with g-$C_{34}N_6$-COF, the adsorption edge of AO-g-$C_{34}N_6$-COF had a slight blueshift.

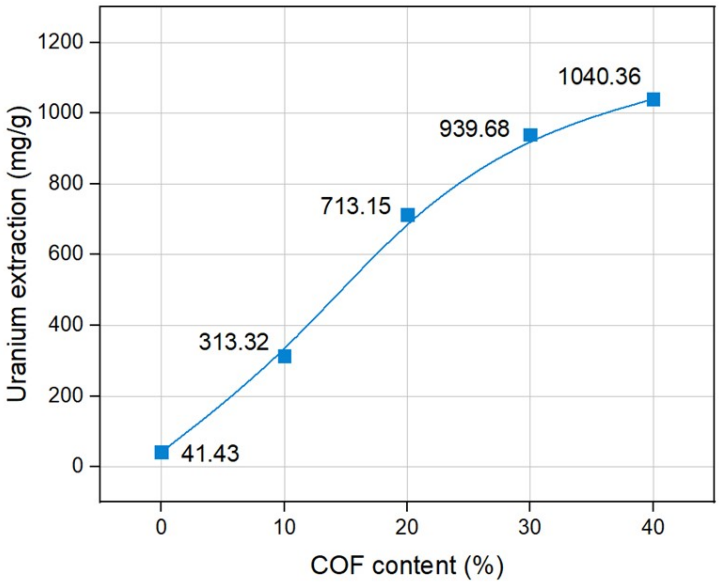

Fig. S11 Uranium extraction performance of S-COF membrane with various content of COF. As COF content rises, the extraction capacity of the membrane improves as well. However, this comes with the trade-off of the membrane becoming more brittle, a consequence of the inherent rigidity of COF fibers.

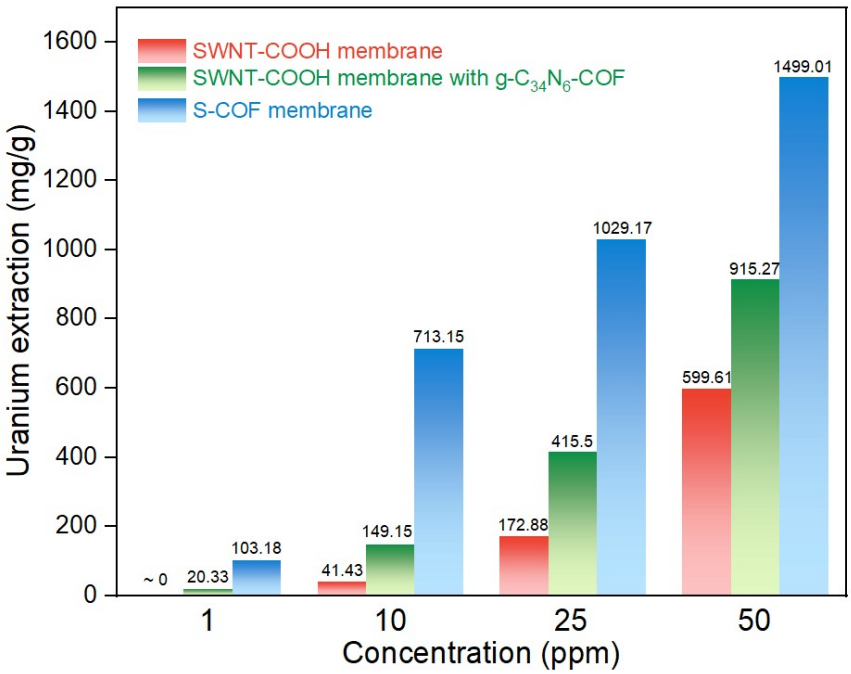

Fig. S12 Uranium extraction performance of SWNT-COOH membrane, SWNT-COOH membrane with g-$C_{34}N_6$-COF and S-COF membrane in seawater with various uranium concentrations. The S-COF membrane had the highest extraction capacity, proving that spontaneous electron transfer cooperates with selective adsorption in complex environments to promote effective uranium extraction.

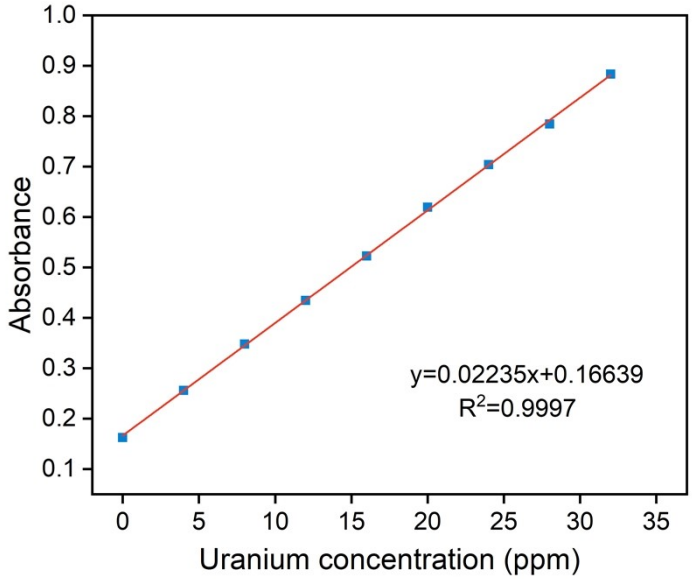

Fig. S13 Standard curve used for determination of uranium concentration. The standard curve was generated from the linear regression fitting of concentration-absorbance in standard solutions with different uranium concentrations. The R^2 of the standard curve is 0.9997.

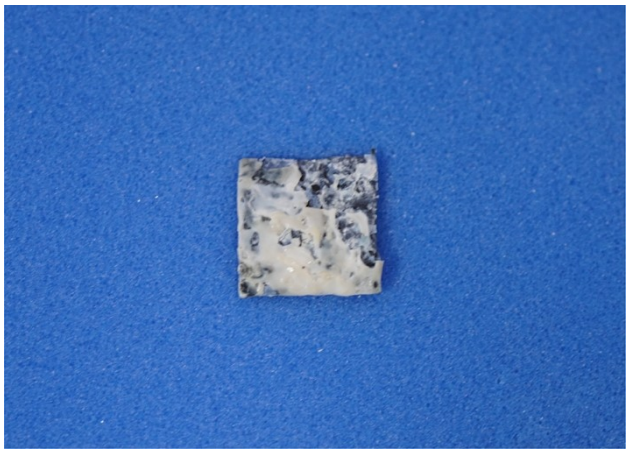

Fig. S14 Digital photo of S-COF membrane after 24-h uranium extraction using a pulse with 4 V amplitude and 75% duty ratio. The deposits had a far slower growth rate than the condition that applies pulse with 5 V amplitude and 75% duty ratio.

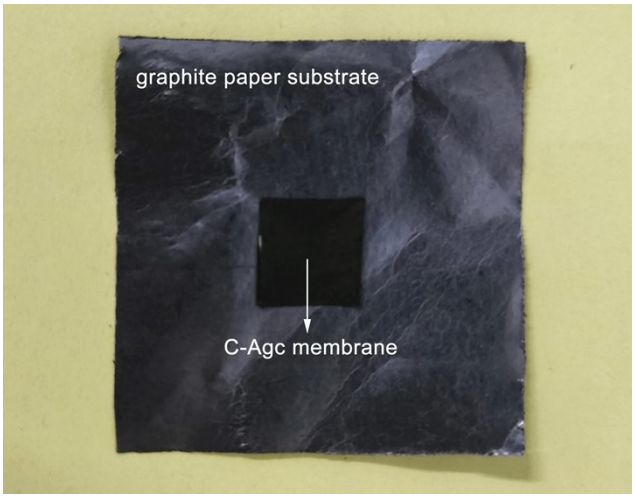

Fig. S15 Digital photo of S-COF membrane composited with graphite paper substrate. The substrates had sizes of 2 cm × 2 cm, 3 cm × 3 cm, and 4 cm × 4 cm. Varying the substrate sizes aimed to control the current density.

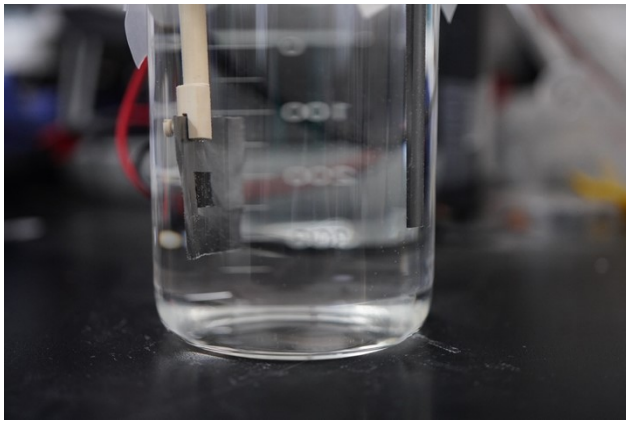

Fig. S16 Digital photograph of test device. The S-COF membrane served as the working electrode, and the counter electrode was a carbon rod. The length of the immersed rod was fixed at 8 cm.

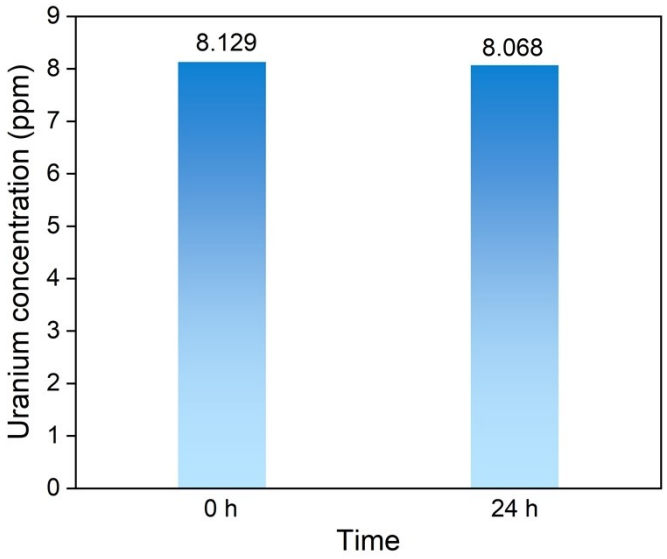

Fig. S17 Uranium concentration in seawater before and after the solution being treated using graphite paper only. When using graphite paper substrate as the working electrode, the uranium concentration was nearly unchanged, illustrating that composing the S-COF membrane with graphite paper would not disturb the estimate of the membrane's uranium extraction performance.

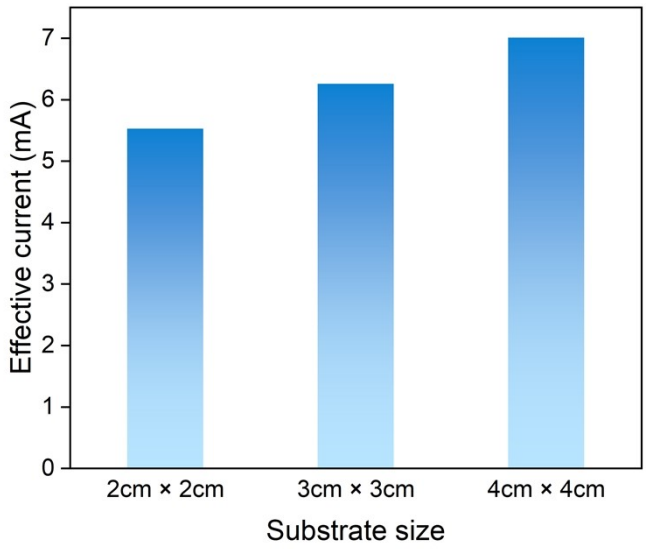

Fig. S18 Instantaneous effective current of composite with different substrate sizes. The instantaneous effective current was measured by a multimeter when the electrode worked for 5 min. The measured current was slightly enhanced when the substrate got bigger in size due to the rise of non-faradaic current.

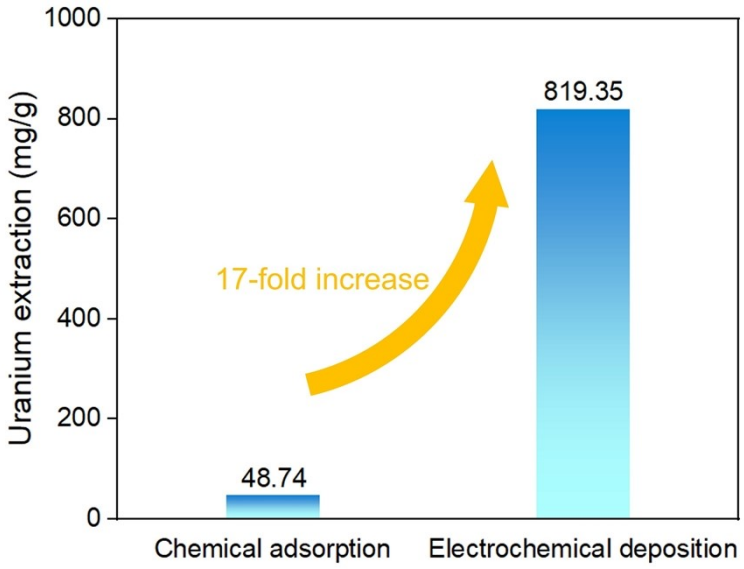

Fig. S19 Uranium extraction amount of S-COF membrane using chemical adsorption and electrochemical deposition methods. The membrane for the electrochemical deposition method had a 17-fold capacity compared to chemical adsorption.

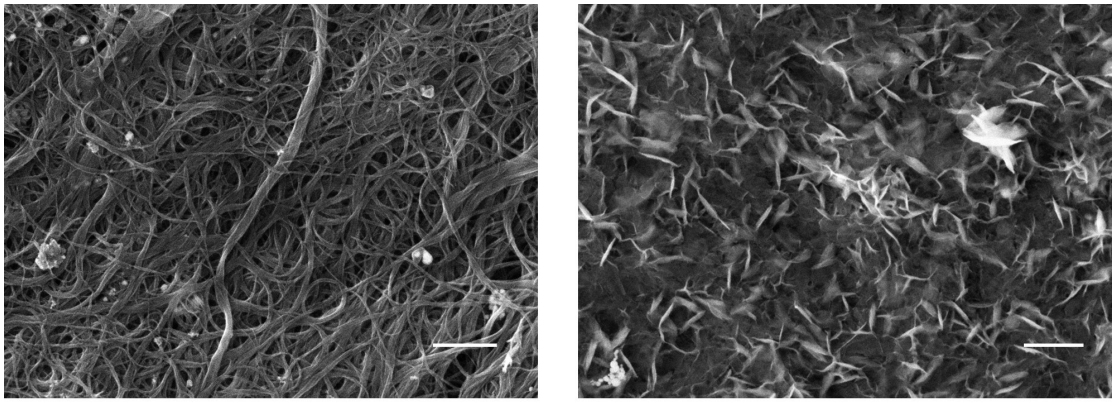

Fig. S20 SEM images of membrane surface after electrochemical uranium extraction with current density regulation (left) and without current density regulation (right). Scale bar, 500 nm.

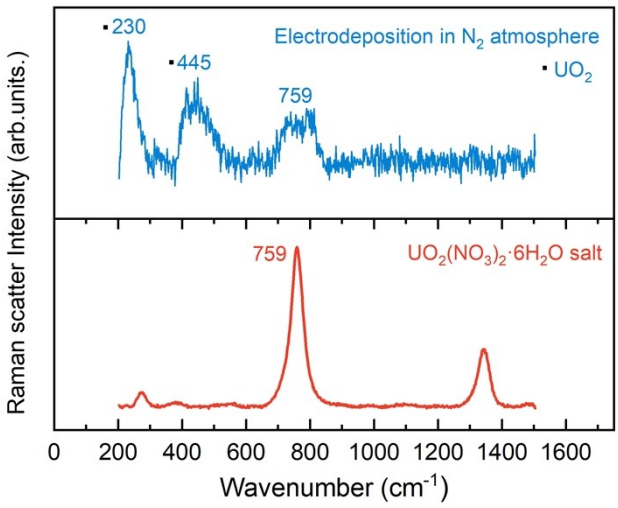

Fig. S21 Raman spectra of $UO_2(NO_3)$·6H2O salt, and products on the S-COF membrane after uranium extraction from aqueous solutions.

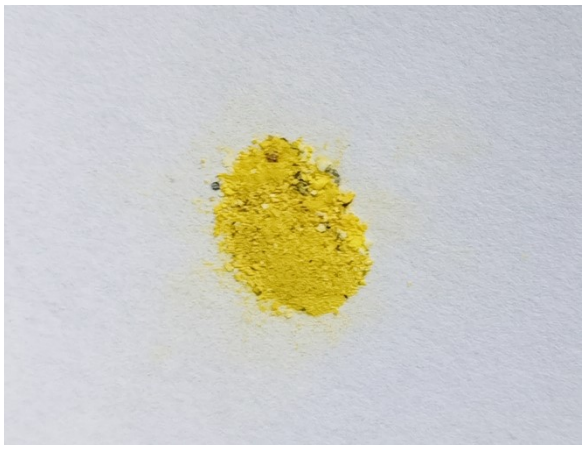

Fig. S22 Digital photo of the electrochemically generated product. The cathodic reduction process yielded yellow powder.

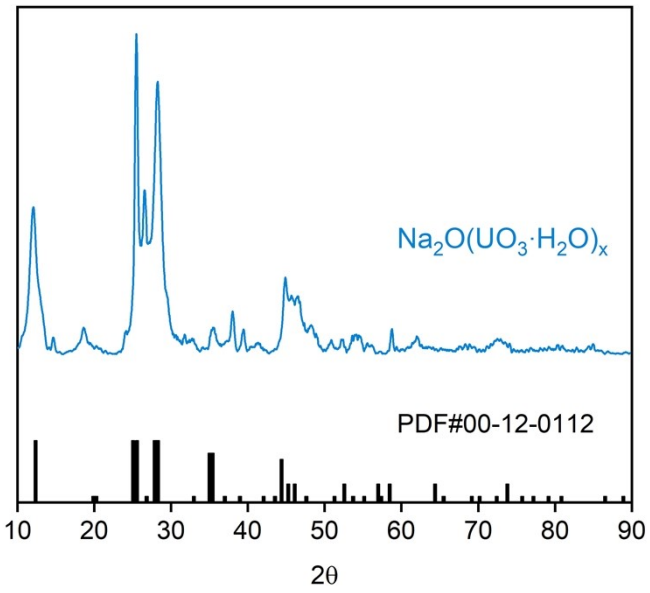

Fig. S23 PXRD pattern of yellow powder generated through cathodic reduction and standard XRD pattern of $Na_2O(UO_3 \cdot H_2O)_x$. The PXRD result illustrated that the product generated through the electrochemical process is $Na_2O(UO_3 \cdot H_2O)_x$.

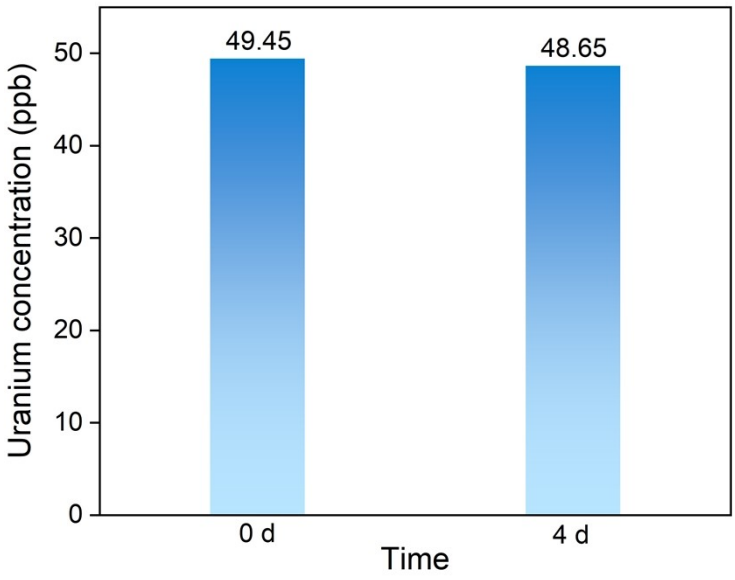

Fig. S24 Uranium concentration in salt lake brine before and after chemical adsorption using S-COF membrane. The membrane displayed an unsatisfactory uranium extraction performance in salt lake brine employing the traditional chemical adsorption method.

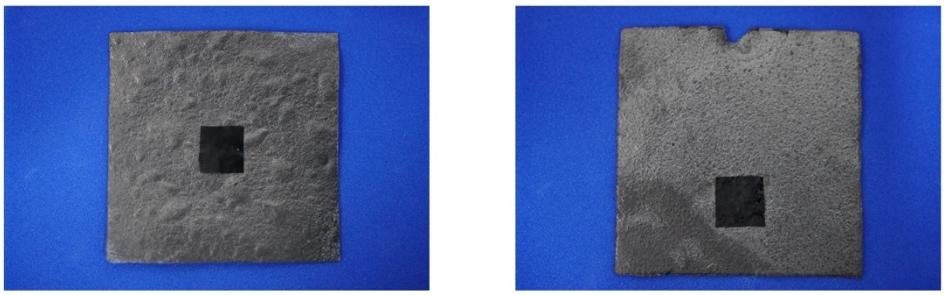

Fig. S25 Digital photos of S-COF electrode after uranium extraction from seawater and salt lake brine. There was no deposit on the surface of the membranes after the electrode extracts uranium from natural seawater and salt lake brine.

Supplementary Tables

Table S1. Fractional atomic coordinates for the unit cell of g-$C_{34}N_6$-COF.

Space group: P1

a = 18.9503 Å, b = 18.1690 Å, c = 3.6499 Å

α = 89.8994°, β = 90.1311°, γ = 118.4068°

Atom	Cartesian coordinates of atoms		
	x	y	z
C1	0.69734	-1.44268	0.42065
C2	0.74237	-1.48558	0.42008
C3	0.82663	-1.43896	0.41947
C4	0.86467	-1.35258	0.41948
C5	0.82023	-1.30849	0.42013
C6	0.73583	-1.35567	0.42069
C7	0.59338	-1.7059	0.42015
N8	0.63789	-1.74567	0.42007
C9	0.71771	-1.69578	0.42006
N10	0.75324	-1.61188	0.41999
C11	0.70398	-1.57784	0.4201
N12	0.62341	-1.62219	0.42028
C13	0.37194	-1.77075	0.42026
C14	0.33692	-1.85882	0.41977
C15	0.38826	-1.89501	0.41947
C16	0.47093	-1.84585	0.41966
C17	0.50528	-1.75828	0.4201
C18	0.45456	-1.72152	0.42039
C19	0.77072	-1.73458	0.42019
C20	0.73917	-1.82208	0.41992
C21	0.78971	-1.85761	0.42009
C22	0.87373	-1.80685	0.42061
C23	0.90461	-1.7193	0.42093
C24	0.85429	-1.68364	0.42067
C25	0.93142	-1.83802	0.4208
N26	0.93584	-2.03636	0.41996
C27	0.9796	-2.07655	0.42017
C28	1.06535	-2.03265	0.42045
C29	1.10664	-1.94393	0.42006
C30	1.05751	-1.90402	0.41952
C31	0.97188	-1.95218	0.41979
C32	1.09754	-1.8152	0.41831
N33	1.13347	-1.74215	0.41717
C34	1.10551	-2.08156	0.42115
N35	1.13437	-2.12586	0.4217

C36	1.25112	1.08496	0.41953
C37	0.91543	1.08097	0.41974
C38	1.19308	1.10845	0.42022
C39	0.85847	0.78237	0.42025
C40	0.93886	0.83276	0.42011
H41	0.63211	-1.47872	0.42109
H42	0.86137	-1.47242	0.41899
H43	0.93	-1.31896	0.41898
H44	0.70047	-1.32264	0.42117
H45	0.33409	-1.74059	0.42045
H46	0.36162	-1.9631	0.41912
H47	0.51035	-1.87406	0.41946
H48	0.48166	-1.65354	0.4207
H49	0.67425	-1.8611	0.41958
H50	0.76408	-1.92555	0.41988
H51	0.96956	-1.6795	0.42132
H52	0.87854	-1.61599	0.42088
H53	0.99342	-1.78855	0.42184
H54	1.2352	1.01896	0.4187
H55	0.85325	1.03113	0.41886
H56	1.21239	1.17539	0.42092
H57	0.81941	0.81135	0.42051
H58	0.97827	0.80451	0.41998

Table S2. Fractional atomic coordinates for unit cell of AO-g-$C_{34}N_6$-COF.

Space group: P1

a = 18.8971 Å, b = 18.3615 Å, c = 4.8936 Å

α = 105.6368°, β = 112.6966°, γ = 118.9138°

Atom	Cartesian coordinates of atoms		
	x	y	z
C1	0.69458	-1.45115	0.38698
C2	0.73948	-1.49357	0.3789
C3	0.82113	-1.44812	0.36076
C4	0.85676	-1.36355	0.35159
C5	0.81229	-1.32019	0.35941
C6	0.73071	-1.36611	0.37813
C7	0.60156	-1.70108	0.44817
N8	0.64663	-1.73987	0.45374
C9	0.72199	-1.69503	0.42516
N10	0.75452	-1.61553	0.40084
C11	0.70479	-1.58198	0.39901
N12	0.62686	-1.62326	0.41783
C13	0.37296	-1.77151	0.41389
C14	0.35346	-1.84119	0.50919
C15	0.41879	-1.86194	0.59126
C16	0.49835	-1.81777	0.56868
C17	0.51718	-1.74857	0.47332
C18	0.45405	-1.72536	0.40029
C19	0.77318	-1.73564	0.41962
C20	0.7467	-1.8169	0.45445
C21	0.79602	-1.85353	0.45165
C22	0.87388	-1.8104	0.41328
C23	0.89976	-1.72905	0.3788
C24	0.85049	-1.69249	0.38086
C25	0.9299	-1.84342	0.40774
N26	0.92663	-2.0469	0.36671
C27	0.96916	-2.08783	0.35497
C28	1.05639	-2.04228	0.36268
C29	1.10188	-1.94974	0.39634
C30	1.06025	-1.9045	0.43478
C31	0.96954	-1.95756	0.40367
C32	1.12106	-1.79869	0.53666
C34	1.09905	-2.09209	0.34623
C36	1.2692	1.10678	0.52603
C37	0.91352	1.07636	0.4105
C38	1.18863	1.10191	0.38813
C39	0.84921	0.77037	0.36109

C40	0.92406	0.81784	0.32994
H41	0.63214	-1.48491	0.40517
H42	0.8568	-1.48019	0.35835
H43	0.92163	-1.32924	0.34647
H44	0.69649	-1.33263	0.3901
H45	0.32465	-1.75272	0.35063
H46	0.40601	-1.9139	0.67393
H47	0.54787	-1.83503	0.62917
H48	0.46972	-1.67093	0.32949
H49	0.68712	-1.85018	0.48644
H50	0.7747	-1.91582	0.48325
H51	0.95946	-1.69496	0.347
H52	0.87071	-1.63014	0.35134
H53	0.99081	-1.79623	0.39627
H54	1.27469	1.07006	0.6658
H55	0.85044	1.0267	0.41012
H56	1.18647	1.14161	0.25814
H57	0.815	0.80246	0.39815
H58	0.95763	0.7855	0.29206
N33	1.18904	1.27108	0.87866
N35	1.1029	1.22169	0.27548
O59	1.24358	1.36995	0.96881
H63	1.03885	1.16029	0.0225
H64	1.16162	1.26263	0.26364
H65	1.20649	1.36614	0.74908
N60	1.07974	0.85979	0.04326
O61	1.12871	0.81988	0.05712
N62	1.16106	0.92102	0.65878
H66	1.19176	0.86367	0.30626
H67	1.14889	0.85786	0.63264
H68	1.16069	0.95376	0.86325

Table S3. Uranium extraction performance of materials based on electrochemical method and performance of various olefin-linked COFs.

	Material	Capacity (mg/g)	Running time	Method
Electrochemical method	This work	48.04	21 d	
	Fe–N–C catalyst[4]	1.2	24 h	
	In–N–C Catalyst[5]	12.7	2 d	
	Fe_3O_4 nanooctahedra[6]	3.49	8 h	
Olefin-linked COFs	This work	48.04	21 d	Electrocatalysis
	BD-TN-AO[7]	5.9	30 d	Photocatalysis
	AF Anti-COF[8]	6.64	28 d	Chemical adsorption
	PT-BN-AO[9]	5.78	27 d	Photocatalysis
	NDA-TN-AO[10]	6.07	27 d	Photocatalysis
	TTh-COF-AO[11]	10.24	30 d	Photocatalysis

Supplementary References

1. J. Xu, Y. He, S. Bi, M. Wang, P. Yang, D. Wu, J. Wang and F. Zhang, *Angew. Chem. Int. Ed.*, 2019, **58**, 12065-12069.
2. S. J. Clark, M. D. Segall, C. J. Pickard, P. J. Hasnip, M. I. J. Probert, K. Refson and M. C. Payne, *Z. Krist.-Cryst. Mater.*, 2005, **220**, 567-570.
3. B. Hourahine, B. Aradi, V. Blum, F. Bonafé, A. Buccheri, C. Camacho, C. Cevallos, M. Y. Deshaye, T. Dumitrică, A. Dominguez, S. Ehlert, M. Elstner, T. van der Heide, J. Hermann, S. Irle, J. J. Kranz, C. Köhler, T. Kowalczyk, T. Kubař, I. S. Lee, V. Lutsker, R. J. Maurer, S. K. Min, I. Mitchell, C. Negre, T. A. Niehaus, A. M. N. Niklasson, A. J. Page, A. Pecchia, G. Penazzi, M. P. Persson, J. Řezáč, C. G. Sánchez, M. Sternberg, M. Stöhr, F. Stuckenberg, A. Tkatchenko, V. W. z. Yu and T. Frauenheim, *J. Chem. Phys.*, 2020, **152**, 124101.
4. H. Yang, X. Liu, M. Hao, Y. Xie, X. Wang, H. Tian, G. I. N. Waterhouse, P. E. Kruger, S. G. Telfer and S. Ma, *Adv. Mater.*, 2021, **33**, 2106621.
5. X. Liu, Y. Xie, M. Hao, Z. Chen, H. Yang, G. I. N. Waterhouse, S. Ma and X. Wang, *Adv. Sci.*, 2022, **9**, 2201735.
6. W. Liu, Y. Yang, R. Cheng, X. Wu, T. Chen, R. He, Y. Liu and W. Zhu, *Sep. Purif. Technol.*, 2023, **319**, 124054.
7. C.-R. Zhang, W.-R. Cui, R.-H. Xu, X.-R. Chen, W. Jiang, Y.-D. Wu, R.-H. Yan, R.-P. Liang and J.-D. Qiu, *CCS Chemistry*, 2021, **3**, 168-179.
8. Y.-D. Wu, W.-R. Cui, C.-R. Zhang, R.-P. Liang and J.-D. Qiu, *Environ. Chem. Lett.*, 2021, **19**, 1847-1856.
9. W.-R. Cui, C.-R. Zhang, R.-H. Xu, X.-R. Chen, R.-H. Yan, W. Jiang, R.-P. Liang and J.-D. Qiu, *ACS ES&T Water*, 2021, **1**, 440-448.
10. W.-R. Cui, F.-F. Li, R.-H. Xu, C.-R. Zhang, X.-R. Chen, R.-H. Yan, R.-P. Liang and J.-D. Qiu, *Angew. Chem. Int. Ed.*, 2020, **59**, 17684-17690.
11. F. Yu, C. Li, W. Li, Z. Yu, Z. Xu, Y. Liu, B. Wang, B. Na and J. Qiu, *Adv. Funct. Mater.*, 2023, 2307230.